Macromolecules
ARTICLE

Macromolecules **2009**, *42*, 4775–4786 **4775**
DOI: 10.1021/ma9002566

Liquid Crystallinity and Other Properties in Complexes of Cationic Azo-Containing Surfactomesogens with Poly(styrenesulfonate)

Qian Zhang and C. Geraldine Bazuin*

Département de chimie, Centre de recherche sur les matériaux auto-assemblés (CRMAA/CSACS), Université de Montréal, C.P. 6128, succursale Centre-Ville, Montréal (QC), Canada H3C 3J7

Received February 4, 2009; Revised Manuscript Received April 22, 2009

ABSTRACT: A series of stoichiometric ionically bonded side-chain polymer complexes, constructed from poly(styrenesulfonate) (PSS) and quaternary ammonium-functionalized azo-containing surfactomesogens (SMs) with hexyl and decyl spacers, were prepared under rigorous conditions and thoroughly dried, and their potential thermotropic liquid crystal (LC) properties were investigated. The SM series consists of eight differently substituted azobenzene cores with a range of polarities. In their Br-neutralized form, they are generally crystalline to high temperatures (those with an ethylamine linking group having very slow recrystallization kinetics). Only some of the complexes showed LC properties in unannealed form, while several others required exceedingly long annealing times at appropriate temperatures to reveal LC character, attributed to the semirigid PS backbone, relatively high molecular weight, and strong ionic interactions that greatly retard the kinetics of chain reorganization toward equilibrium. Among the decyl-spacer complexes, only the two with an ethylamine linking group appear intrinsically isotropic, whereas, among the hexyl-spacer complexes, just two revealed LC character. X-ray diffraction (XRD) indicated that the LC structure is generally of an effectively single-layer SmA type, but while the complexes based on SMs with nonpolar tails produce a classical SmA XRD pattern, those with polar tails produce one with a quasi-extinct or reduced intensity first-order diffraction peak. The former also have lamellar thicknesses that are ca. 5 Å less than the latter, in agreement with literature data for all-covalent polystyrene-based analogues and explained by greater mesogen interdigitation for those with nonpolar tails that thus lie in the alkyl spacer subplane. A model proposed to rationalize the apparent extinction of the first-order XRD peak relies on dipole−dipole interactions between the polar mesogens and the ion pairs that allow them to share the same subplane, thus halving the effective lamellar thickness. A study of photoinduced birefringence (PIB) in selected complexes, compared with a spacer-free complex, shows that the flexible spacer plays a significant role in reducing PIB stability.

Introduction

Azo-containing polymers are of great interest for potential applications as optically driven functional materials, based on the reversible trans−cis photoisomerisation of the azo bond (see, for example, reviews 1−6). When combined with liquid crystal (LC) character, optical control can be further enhanced by exploiting the inherent anisotropy of LC materials.[2] Elegant illustrations of the latter are based on the photomechanical effect, such as observed in directed light-induced bending of azo-based LC polymer films[7] and a light-driven plastic motor.[8]

To simplify synthetic procedures, yet avoid the problematics of doped systems, supramolecular means to obtaining azo-containing and LC polymers (LCPs) are attractive.[9−14] Supramolecular thermotropic LCPs, some of which are azo-containing, have been investigated extensively for more than a decade (see, e.g., reviews 15−22) and continue to be studied (see, e.g., refs 23−27, to mention only homopolymer systems). The majority utilize hydrogen bonds as supramolecular links, within both main-chain and side-chain architectures. Ionic bond systems are usually in the form of side-chain LCPs (SCLCPs) and most frequently involve alkyl surfactants complexed to oppositely charged polyelectrolytes. There are fewer papers on ionically complexed SCLCPs derived from molecules that combine a surfactant-like structure (ionic headgroup and alkyl chain) with a thermotropic mesogen structure (elongated aromatic core and alkyl chain),[12,18,28−32] termed surfactomesogens[32,33] and illustrated in Scheme 1. Of these, none have compared the LC properties of such complexes that involve a series of different mesogenic motifs, a kind of comparison that is limited even in all-covalent SCLCPs. It should be noted, however, that surfactomesogens have been studied in solution and in ultrathin films (Langmuir−Blodgett, layer-by-layer), where they are often complexed with polyelectrolytes or surfactants, and also occasionally in the bulk state (see, e.g., refs 6, 21, and 34−42). Similar compounds have been used to construct SCLCP systems based on H-bonding,[15−17,43] but these interactions are sometimes too weak to lead to high complexation rates, in particular when the driving force for self-crystallization of the mesogenic molecules is strong, which can compromise the ability to obtain LC properties in the complexes.[44,45]

Ionically complexed LCPs present greater challenges than hydrogen-bonded systems. Ionic bonds are generally stronger and require higher temperatures to become labile compared to H-bonds, leading to highly viscous melts, which can result in frozen-in kinetic structures. Furthermore, as is well-known for solid-state polyelectrolytes and ionomers, ion-containing systems are susceptible to the presence of (trace) amounts of water and are often insufficiently dried or even impossible to dry completely without some degradation.[46,47] Even if well-dried, they may be subject to rapid absorption of ambient humidity during sample

*To whom correspondence should be addressed. E-mail: geraldine.bazuin@umontreal.ca.

Published on Web 06/18/2009

Scheme 1. Representation of the Ionic Complex, SM/PSS, Obtained from a Surfactomesogen (SM-Br) and an Oppositely Charged Polyelectrolyte, Poly(sodium styrenesulfonate) (PSS−Na), with Elimination of the NaBr Counterions

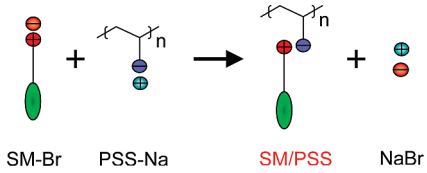

preparation or transfer to the measuring device, particularly on humid days. On the other hand, strong ionic complexation is attractive for obtaining robust supramolecular systems,[18,28] for possibly mitigating the plasticizing effect of side chains,[48] and thus for designing higher performance materials.[20]

In the present study, we investigate the thermotropic properties of a series of triethylammonium-functionalized surfactomesogens with azo-containing mesogenic cores that are complexed to a readily available oppositely charged polyelectrolyte, poly(sodium styrenesulfonate) (PSS-Na), paying particular attention to the above factors.[49] We also briefly examine photoinduced birefringence in selected complexes. The sulfonate functionality of PSS-Na is known to lead to strong cooperative binding in polyelectrolyte−surfactant solutions.[20,34] The polystyrene backbone may enhance the rigidity and increase the glass transition temperature (T_g) of the complexes,[50−52] an advantage for the long-term stability often required for electro-optical applications.[53−55] The linear alkyl chain spacer between the mesogenic core and ionic moiety of the surfactomesogens is composed of 6 and 10 carbons, as representative of two commonly used spacer lengths in all-covalent SCLCPs.[56,57] The substituents of the mesogenic azo core, along with the nomenclature used and the core dipole moments, are listed in Table 1. A number of analogous all-covalent azo-containing SCLCPs based on polystyrene, particularly with O_2N-O, H_3CO-O, and NC−O mesogenic motifs with different spacer lengths, have been investigated in the past,[50,52,53,58−66] providing a convenient point of comparison for the present complexes.

Experimental Section

Synthesis of Surfactomesogens. The SMs were synthesized using well-known procedures,[68,69] as indicated in Scheme 2 for (a) the phenol type and (b) the aniline type families. The synthesis of O_2N-OnQ was reported previously.[36] Those of the azophenol derivatives and several of the alkyl bromide-substituted precursors, in particular as intermediates in the synthesis of other azo molecules and SCLCPs, have also been reported elsewhere (see, e.g., refs 25, 58−60, 70, 71, and many citations in refs 1−21). The particular procedures followed by us for a representative phenol-type and a representative aniline-type SM, along with the elemental and molecular characterization of all of the SMs, are given in the Supporting Information.

Preparation of the SM/PSS Complexes. The polyelectrolyte used, poly(sodium 4-styrenesulfonate) (PSS-Na), was obtained from Sigma-Aldrich [MW = 70 000 and Brookfield viscosity 15 000−55 000 cps in 20% solution at 25 °C, reported by the supplier; M_n = 45 000 (DP_n ca. 220) and M_w/M_n = 2.0, determined in ref 32]. The SM/PSS complexes were prepared by ion-exchange procedures (Scheme 1) as follows. The SM was dissolved in DMSO (spectrograde; Sigma-Aldrich) at a concentration of ca. 40 mg/mL. In parallel, PSS was dissolved in a minimal amount (a few drops) of deionized water (Millipore) giving a clear gel-like solution, to which DMSO (ca. 1 mL per 20 mg of PSS) was then added. The amounts of PSS and SM used were calculated to have a small excess (2−5 mol %) of SM relative to the PSS repeat unit, to optimize for stoichiometric

Table 1. Nomenclature of the Azo-Containing Surfactomesogens (SMs) Synthesized[a] and Calculated Dipole Moments of the Mesogen Core[b]

	phenol type	aniline type		
surfactomesogen (SM)	X	Y	Z	dipole moment (D)
$O_2N-N(Et)nQ$		NO_2	CH_2CH_3	10.00
$O_2N-N(Me)nQ$		NO_2	CH_3	9.96[d]
$NC-N(Et)nQ$[c]		CN	CH_2CH_3	8.74
O_2N-OnQ	NO_2			7.49
NC−OnQ	CN			5.57
$H_3CO-OnQ$	OCH_3			0−3[e]
H_3C-OnQ	CH_3			2.00
H−OnQ	H			1.76

[a] The hyphen designates the azobenzene core, *n* refers to the linear spacer composed of *n* = 6 and 10 CH_2 groups, and Q refers to the triethylammonium head group. The SMs are neutralized by Br (SM-Br) or, when complexed, by PSS (SM/PSS). The azobenzene substituents X, Y, and Z are indicated in Scheme 2. [b] The dipole moments of the mesogenic core in trans form, with *n*Q replaced by CH_3, were calculated using Hyperchem 7. [c] Only *n* = 10 was synthesized. [d] In agreement with the value of 9.94 D in ref 67. [e] Calculated values are subject to the molecular conformation: it is 0 D when the methoxy groups are on opposite sides of the azobenzene axis (symmetric conformation) and 3.42 D when the methoxy groups are on the same side of the azobenzene axis (antisymmetric conformation).

Scheme 2. General Synthetic Strategy of the Azo Surfactomesogens (SM-Br): (a) Phenol Type and (b) Aniline Type

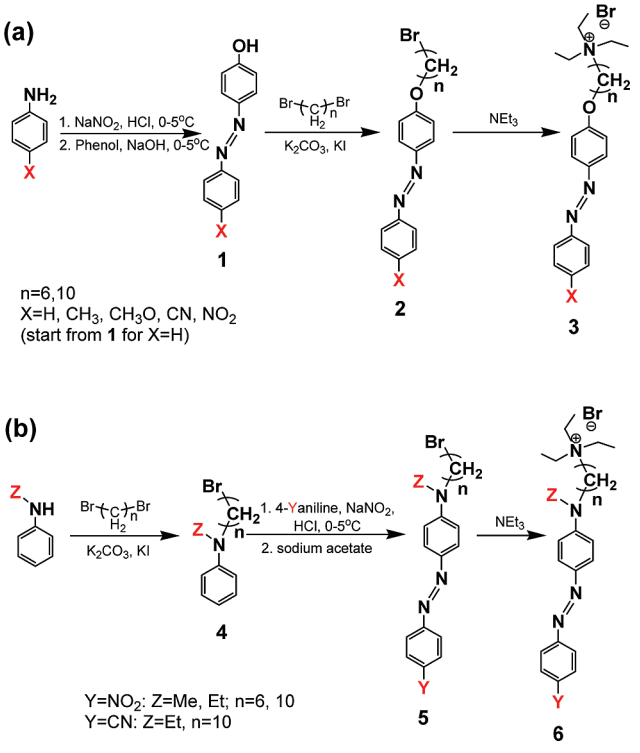

complexes, given that excess SM is easily eliminated during the subsequent dialysis procedure. The two separately prepared solutions were stirred in a 60 °C oil bath for ca. 15 min, and then the SM solution was added dropwise to the PSS solution (with DMSO rinsing). If precipitation occurred, enough DMSO was added until resolubilization occurred (to facilitate removal of counterions and excess SM during dialysis). The final concentration of the transparent, colored solution was typically ca. 35 mg/mL. It was stirred at 60 °C for 24 h and then transferred to a dialysis bag (Spectrapor, cutoff MW 3500; VWR) where it was dialyzed for a minimum of 4 days against deionized water (ca. 3 L) that was refreshed at least once a day. In the course of

Table 2. Thermal Properties of the Azo Surfactomesogens, SM-Br, Determined by DSC and TGA[a]

	T_m/°C (ΔH/J g^{-1})		T_{cr}/°C (ΔH/J g^{-1})		$T_d^{1\%}$/°C	
sample[b]	6Q	10Q	6Q	10Q	6Q	10Q
$O_2N-N(Et)$	207 (> 45[d])	132 (88), 147 (2)[f]	(max 210)	(max 153)	199	179
	188 (48)	T_g = 41[g]	144 (−50)	T_g = 30[g]		
$O_2N-N(Me)$	188 (61)	163 (85)	(max 195)	(max 175)	192	184
	184 (53)	132 (46)	166 (−60)	105 (−44)		
NC−N(Et)		101, 108 (39)[h]		(max 118)		154
		T_g = 38[g]		T_g = 27[g]		
O_2N-O[c]	166 (86)	141 (62)	(max 185)	(max 150)	177	173
	163 (71)	142 (28)	124 (−72)	115 (−25)		
NC−O	171 (94), 182 (55)[e]	154 (86)	(max 190)	(max 170)	187	182
	167 (75)	153 (84)	126 (−58)	114 (−76)		
H_3CO-O	195 (148)	186 (185)	(max 205)	(max 195)	193	186
	188 (112)	181 (119)	93 (−8)	140 (−124)		
H_3C-O	163 (68)	174 (85)	(max 170)	(max 180)	184	182
	163 (61)	173 (81)	122 (−59)	127 (−89)		
H−O	157 (95)	178 (81)	(max 165)	(max 185)	190	188
	157 (94)	176 (75)	109 (−82)	146 (−77)		

[a] The DSC (first heating) and TGA thermograms are given in the Supporting Information. The melting points (T_m, peak values) and enthalpies (ΔH) are from the first (upper entry) and second (lower entry) DSC heating scans. The crystallization temperatures (T_{cr}), obtained from the intermediate DSC cooling scan, are accompanied by the maximum temperature (max) of the first heating scan. T_m and T_{cr} are the maxima/minima of the peaks. $T_d^{1\%}$ is the temperature of 1% weight loss relative to the weight at 80 °C. [b] The sample identification indicates the terminal and linking groups on either side of the azobenzene core. [c] The $O_2N-O10Q$ SM was synthesized three times, each batch giving identical DSC data. In subsequent heating scans, a transition appeared at 124 °C that increased in intensity at the expense of the peak at 141 °C with each scan (cooling scan unchanged). [d] Scan stopped before baseline reached. [e] Recrystallization appears to occur between the two sharp peaks (exothermic dip). [f] The two temperatures given are the most intense and the highest temperature peaks, respectively, of multiple peaks. [g] No crystallization was observed in subsequent scans following melting; the T_g's given are inflection point values. [h] Two partially overlapping peaks of similar intensities.

dialysis, the resulting complex formed a precipitate and/or a colloidal suspension inside the dialysis bag. The bag contents were transferred to a freeze-drying flask for several days of freeze-drying, followed by vacuum-drying at ca. 60 °C for a week, and then storage in a desiccator containing drierite (Sigma-Aldrich). The elimination of all detectable sodium bromide counterions was verified by EDS. The elemental and molecular characterization of the complexes is given in the Supporting Information. For one complex, it was verified that ca. 3 days of dialysis is sufficient to obtain pure stoichiometric complexes and that this is unchanged by longer dialysis times.[72] Just before measurement, the samples were again vacuum-dried overnight at ca. 60 °C. Many samples were annealed for POM and XRD studies; in this case, they were annealed in the microscope slides and sealed XRD capillaries, respectively, placed in a hot stage (Mettler FP5 or Linkam TMS94).

Instrumentation. ^{1}H NMR (500 MHz) spectra were obtained using a Bruker Avance spectrometer and mass spectral data using an Agilent Technologies 6210 time-of-flight LC/MS spectrometer. CHNS elemental analysis was done using a Fisons AE1108 analyzer, Na^+ and Br^- analysis using a FEI Quanta 200 FEG environmental scanning electron microscope equipped with an energy dispersive spectrometer (EDS), and thermogravimetric analysis (TGA) using a TA Instruments Hi-Res TGA 2950 analyzer at a heating rate of 10 °C/min under a nitrogen atmosphere. Differential scanning calorimetry (DSC) was performed using a TA Instruments Q1000 DSC at heating and cooling rates of 10 °C/min and polarizing optical microscopy (POM) using a Zeiss Axioskop 40Pol microscope coupled with a Linkam Scientific Instrument THMS600 hot stage and a TMS94 temperature controller. X-ray diffraction (XRD) analysis on powder-like samples packed in 1.0 mm diameter glass capillaries (Charles Supper) was performed with a Bruker D8 Discover system equipped with a 2D Bruker AXS wire-grid detector, using Cu Kα radiation; sample temperature was controlled by a modified Instec HCS410 heating stage and STC200 temperature controller. UV−vis spectra of well-dried films spin-coated from DMF for O_2N-OnQ/PSS and from DMSO for $O_2N-N(Et)10Q$/PSS were obtained using a Varian Cary 500 Scan UV−vis−NIR spectrophotometer. Freeze-drying was effected using an FTS Systems FD-3-85A-MP freeze-dryer working at 1−3 mT with the condenser at −90 °C. The molecular dipole moment of the trans mesogenic core (with a methyl group replacing the ammonium-capped alkyl spacer) was calculated by HyperChem 7.0 (Hypercube), using the ab initio procedure with a small basis set (3-21G) and the conjugate gradient method with an rms gradient of 0.1 kcal/(Å mol) as the termination condition. The most extended molecular lengths (l_c) of the SMs and SM/PSS repeat units (with van der Waals radii at the extremities included) were estimated by Hyperchem 7.0 energy minimization simulations. For the complexes, the ionic groups were placed in close proximity lying either along the molecular long axis or laterally relative to the long axis before applying minimization.

Photoinduced Birefringence (PIB). Photoinduced birefringence in spin-coated films of several complexes was examined using a 454 nm Ar ion writing laser at a power of ca. 700 mW/cm^2 using the same setup as in ref 9. The $O_2N-N(Et)$ 10Q/PSS and $O_2N-O10Q$/PSS films were spin-coated from dichloromethane (6.6 and 11.6 wt % concentration, respectively) and the O_2N-O6Q/PSS film from nitromethane/dichloromethane (0.74/1 w/w, 11.6 wt % concentration). They were dried in a vacuum oven at 80 °C for at least 1 week. The films were estimated to have a thickness of the order of 0.5 μm. The sample chamber was flushed with dry N_2 during PIB measurements.

Results and Discussion

Characteristics of the Surfactomesogens (SM-Br). The SM-Br, having been subjected to rigorous column chromatography and crystallization purification procedures, are highly pure, as attested to by NMR and elemental analysis.[72] Their thermal properties determined by DSC and TGA are summarized in Table 2. Their 1 wt % loss values ($T_d^{1\%}$) generally lie between ca. 175 and 200 °C (usually slightly higher for the 6-spacer than the 10-spacer ones), with only NC−N(Et)10Q significantly lower (at 155 °C).

All but two of the surfactomesogens are crystalline to high temperature, ranging from ca. 140 to 210 °C, where they melt directly to the isotropic phase, and recrystallize with a supercooling of typically 30−50 °C (keeping in mind that the data obtained after melting may be affected by slight degradation in the cases where the maximum scan

temperature was near or beyond $T_d^{1\%}$). Usually, the 6-spacer SM-Br has a higher melting point than the corresponding 10-spacer SM-Br. The two lower melting compounds, NC−N(Et)10Q (which has a double melting peak in the 100−110 °C range)[72] and O_2N−N(Et)10Q (which has a complex melting pattern in the 120−150 °C range),[72] do not recrystallize at all in the DSC conditions after melting but instead show an apparent glass transition near 40 °C in subsequent heating scans (in these two cases, the maximum temperature scans were well below $T_d^{1\%}$). However, POM and XRD investigations showed that crystallization occurs very slowly in these compounds [more slowly for NC-N(Et)10Q than for O_2N−N(Et)10Q] during annealing, performed at ca. 95 °C for several hours. No evidence of a liquid crystal mesophase in this region could be found by POM or XRD.

The ambient-temperature diffractograms of the SM-Br before melting prove their crystalline character.[72] The presence of two and sometimes three (most often for the 10Q SMs) lower-angle equidistant diffraction peaks for the majority of the compounds are indicative of lamellar stacking. The spacings deduced from the peaks are usually significantly smaller than the calculated molecular lengths of the surfactomesogens in extended conformation,[72] suggesting that these molecules are tilted relative to the layer normal. Single crystals were obtained for H_3CO−O6Q and O_2N−O10Q, and XRD analysis indicates a triclinic crystal system for both.[72]

Table 3. Thermal Properties of the SM/PSS Complexes, Determined by DSC and TGA

	T_g[a] (°C)		T_{cl}[b] (°C) (ΔH) (J g^{-1})		$T_d^{1\%}$[c] (°C)	
SM	6Q	10Q	6Q	10Q	6Q	10Q
O_2N−N(Et)*n*Q	97	69			240	225
O_2N−N(Me)*n*Q	95	70	155 (1) *140 (−1)*	∼120	241	241
NC−N(Et)10Q		72				238
O_2N−O*n*Q	81	46		165 (1) *156 (−1)*	243	241
NC−O*n*Q	88	68		∼120 (≪1)	253	252
H_3CO−O*n*Q	76	55		136 (9) *128 (−7)*	262	243
H_3C−O*n*Q	70	45		95 (2) *84 (−2)*	258	240
H−O*n*Q	71	51		113 (3) *105 (−3)*	267	253

[a] The T_g data (inflection points) are from the second and higher DSC heating scans (identical); the first heating scans generally show a very broad endotherm in this region. All ΔC_p's lie in the 0.2−0.3 J g^{-1} °C^{-1} range. [b] The T_{cl} data are maximum/minimum peak values (identical in multiple scans), obtained from the DSC heating and *cooling (in italics)* curves. [c] TGA data, relative to the weight at 80 °C.

General Characteristics of the SM/PSS Complexes. The surfactomesogen/PSS complexes were all ascertained to be stoichiometric with respect to the ionic moieties, according to elemental analysis (CHNS data; absence of Na and Br signals in EDS data) and NMR.[72] For some complexes, conductivity measurements of the dialyzed mixture were also effected: the very low values measured (< 10 uS/cm generally[72]) are consistent with the quasi-absence of mobile small counterions and with the insolubility—i.e., lack of mobility—of the complexes in H_2O. The complexes are not only insoluble in H_2O, in common with stoichiometric surfactant/polyelectrolyte complexes,[34,73,74] but also in most other common solvents including alcohols (except at low concentrations). DMSO and DMF are the only readily available solvents for all of the complexes. Pyridine dissolves O_2N−N(Et)10Q/PSS, O_2N−O10Q/PSS, and O_2N−O6Q/PSS, whereas dichloromethane dissolves the first two but not the last of these three complexes unless nitromethane is added (the other complexes were not tested in these solvents).

Thermal and Birefringence Properties of the SM/PSS Complexes. The 1% weight loss ($T_d^{1\%}$) values of the complexes measured by dynamic TGA lie, with one exception, between ca. 240 and 270 °C (Table 3). Thus, the complexes are 50−80 °C more stable thermally than the corresponding Br-neutralized surfactomesogens. The maximum temperatures reached in the investigations of these complexes are well below the $T_d^{1\%}$ values.

DSC thermograms of the complexes are shown in Figure 1, with extracted data given in Table 3. Contrary to the SM-Br, none of the complexes display any crystallinity (see also XRD data below); instead, a well-defined glass transition and, in some cases, a first-order transition peak are evident. These features are general for many (stoichiometric) ionically complexed SCLCPs;[28−32] however, given the series of mesogens investigated here, a number of specific observations and trends can be pointed out.

First, the T_g of the complexes lies between 45 and 100 °C, with that of the 6-spacer one being about 25 ± 5 °C higher than that of the corresponding 10-spacer one. The internal plasticization effect of the alkyl spacers is thus about 6 ± 1 °C/CH_2, as also found for tail-end pyridinium alkyl polymethacrylate comblike homopolymers.[48,75] For the same spacer length, the aniline-type SM/PSS complexes, all with polar end groups, have almost identical T_g's, which thus

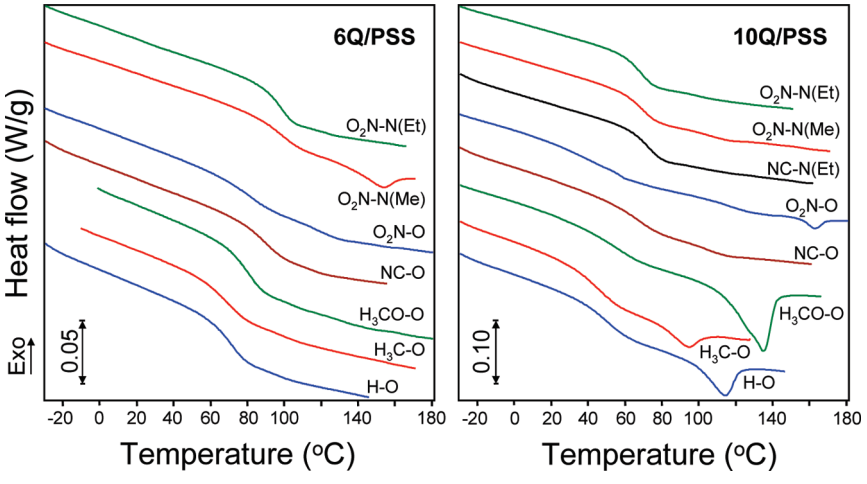

Figure 1. DSC thermograms (second heating curves, 10 °C/min) of the SM/PSS complexes.

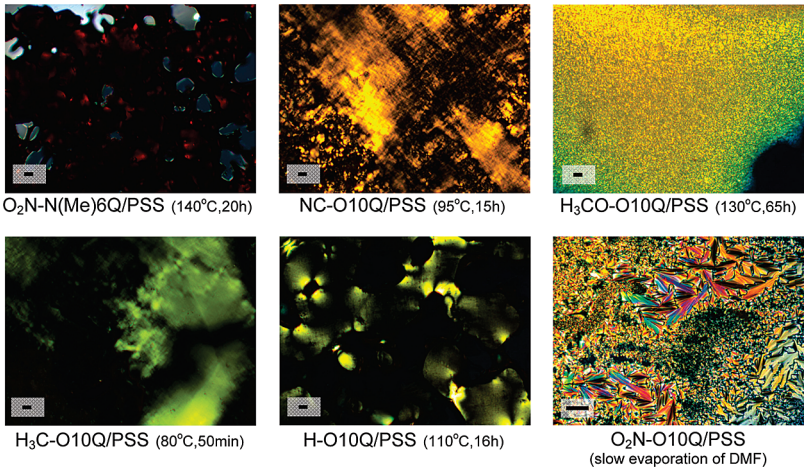

Figure 2. Polarizing optical micrographs of selected complexes taken after cooling from the isotropic phase at the temperatures and annealing times indicated. In the lower right picture, the complex was dissolved in DMF and the texture developed during slow solvent evaporation. The scale bar represents 20 μm.

appear to be independent of the nature of the lateral substituent on the amine (Me or Et) and of the polar end group (CN or NO_2). Furthermore, the T_g's of the aniline-type complexes are higher than or equal to those of the phenol-type complexes. This can be attributed to the higher polarity of the aniline-type mesogens and to the greater bulkiness (branched structure) of the laterally substituted amine compared to the ether linking group. Of the phenol-type complexes, the one with the polar cyano tail has the highest T_g for both 6Q and 10Q, whereas those with a nonpolar tail (H, CH_3, OCH_3) have the lowest T_g's. Overall, except for $O_2N-O10Q/PSS$, the T_g tends to follow the dipole moment value of the SM azo groups, which is the highest and very similar for the three aniline-type SMs and the lowest and very similar for the three phenol-type SMs with a nonpolar end group (see Table 1). The coherency of the above data relative to their molecular characteristics concords with the quality of the complexes as established by their molecular and elemental analyses.

In comparing the T_g's of the complexes with all-covalent PS-based analogues (see Supporting Information), it is found that those of the complexes are sometimes higher, sometimes similar, and sometimes lower than those of the all-covalent analogues, which does not seem to be related to a molecular weight effect.[59,61,63,65] The only correlation that can be drawn between the presence of ionic interactions and the T_g in these PS-based SCLCPs is the following (based on three mesogen types only): the ones with polar end groups (CN and NO_2) give a higher or similar T_g in the complexes than in the all-covalent analogues, whereas the one with the nonpolar end group (CH_3O) gives a lower T_g in the complexes than in the all-covalent analogues.

A distinct first-order transition, shown by POM (Figure 2) and XRD (see later) to be a clearing temperature (T_{cl}) from a birefringent liquid crystalline phase to the isotropic phase, is apparent in the heating and cooling DSC thermograms of only four out of the eight 10Q complexes ($H-O10Q/PSS$, $H_3C-O10Q/PSS$, $H_3CO-O10Q/PSS$, $O_2N-O10Q/PSS$; all in the phenol family) and one 6Q complex [$O_2N-N(Me)6Q/PSS$; in the aniline family]. Of the four 10Q complexes, the transition occurs at the highest temperature for the one with the polar NO_2 tail compared to the three with the nonpolar tails, as observed also for the analogous PS-based SCLCPs (154 °C[63] vs 141 °C[61] for NO_2 vs CH_3O tails).

For the five complexes showing a clear T_{cl} in DSC, reversible birefringence was observed by POM for the four 10Q complexes but, surprisingly, not for the 6Q complex. (Since the complexes are highly absorbing and also very difficult to spread by application of pressure even at high temperatures, it is generally restricted to thin parts of the samples.) Generally, the birefringence tends to brighten after some time of annealing above the T_g. Among the three phenol-type 10Q complexes with a nonpolar end group, birefringence becomes brighter and maximum birefringence reached with shorter annealing time in the end-group order $H_3CO \gg H > H_3C$, which is the same order found for the ΔH and T_{cl} values (Table 3). This relation may be intrinsic to the type of complex, but it may also reflect differing "degrees of liquid crystallinity", as discussed later.

Revelatory POM textures were impossible to develop in these samples either by lengthy annealing a little below T_{cl} (see examples in Figure 2) or by very slow cooling ($\leq$0.2 °C/min) from the isotropic phase. By comparison, identifiable textures for all-covalent PS-based SCLCPs were also reported to be impossible to obtain by annealing[58,60,61] (in contrast to SCLCPs based on more flexible backbones[76]); however, they were obtainable by very slow cooling from the isotropic phase.[50,60,61,63] Clearly, the rigid PS backbone must be a significant hindrance to texture formation in the complexes, but this is no doubt exacerbated by both the much higher MW of the present complexes compared to the PS-based SCLCPs as well as by the strong ionic interactions, which are well-known to retard, often drastically, the onset of flow in ionomers.[46]

The only way found to develop a revealing POM texture in the complexes, tested only on $O_2N-O10Q/PSS$, was by applying a solvent-assisted technique used to obtain LC textures in block copolymers[77]—notably, dissolution of the complex in dilute DMF (< 1 wt %), followed by solvent-casting on a glass slide, slow solvent evaporation over a period of 2 weeks at ambient temperature, and thorough drying in a vacuum oven at ca. 100 °C. This produced a focal-conic fan-shaped texture in a very small portion of the film, shown in Figure 2 (the rest of the film was birefringent, but with no specific texture), and suggestive of a SmA mesophase as observed in other ionically complexed SCLCPs.[9,28−32] However, it may be argued that the focal-conic texture was formed and frozen in from a concentrated lyotropic solution.[49]

Although the other 10Q complexes displayed no obvious birefringence in POM, some of them show hints of additional thermal events in the DSC curves above the

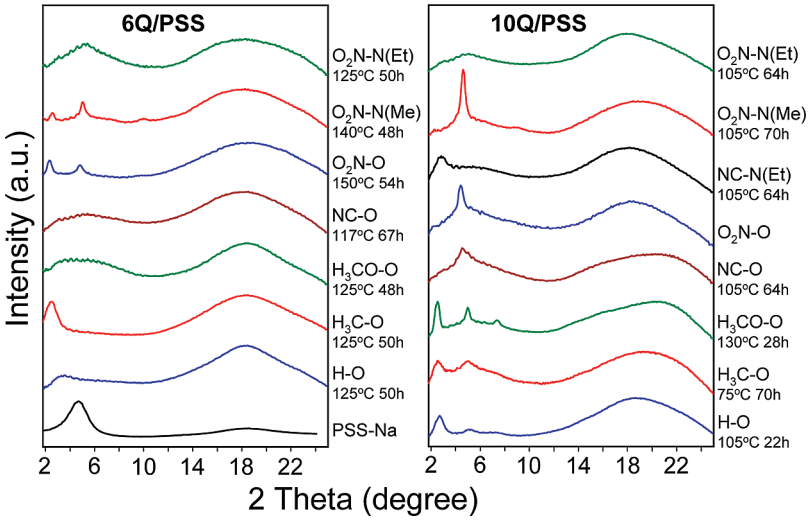

Figure 3. Ambient temperature X-ray diffractograms of the 6Q/PSS and 10Q/PSS complexes, with preceding annealing temperatures and times indicated. That for $O_2N-O10Q$ was obtained after a heating and cooling cycle of diffractograms taken at various temperatures (maximum 195 °C; see Supporting Information for the complete cycle). A diffractogram of PSS−Na is included.

Table 4. Angles in 2θ and Corresponding Bragg Spacings, *d*, of the XRD Diffraction Peaks for the SM/PSS Complexes and PSS-Na,[a] Determined from the Diffractograms in Figure 3, and Calculated Molecular Lengths for the Ion Pairs in Serial (l_A) and Side-by-Side (l_B) Arrangement

	6Q/PSS				10Q/PSS			
complex	2θ (deg)	*d* (Å)	l_A (Å)	l_B (Å)	2θ (deg)	*d* (Å)	l_A (Å)	l_B (Å)
$O_2N-N(Et)$	(5.4)	(16.3)	34.1	29.4	(5.1)	(17.3)	38.3	34.5
$O_2N-N(Me)$	2.56	34.5	34.1	29.3	4.63	19.1	38.2	33.6
	5.07	17.4			9.12	9.7		
	9.97	8.9						
NC−N(Et)					(2.8)	(31.5)	38.4	33.3
O_2N-O	2.40	36.8	35.9	29.6	4.44	19.9	40.9	35.8
	4.90	18.0						
NC−O			36.1	32.0	4.66	19.0	41.1	36.5
H_3CO-O			36.5	31.8	2.51	35.1	41.5	35.9
					5.01	17.6		
					7.41	11.9		
H_3C-O	(2.5)	(35.3)	35.6	31.6	2.62	33.7	40.6	35.5
					5.09	17.4		
H−O	(3.4)	(26.0)	34.6	30.9	2.72	32.5	39.6	34.3
					5.19	17.0		
					7.4	11.9		
PSS−Na	4.64	19.0						

[a] Data in parentheses are for broad peaks, considered to arise from short-range order in an otherwise isotropic state.

T_g (Figure 1): these events, which are reproducible in multiple scans, may be very weak broad peaks, may correspond to a second T_g-like event as observed previously in some other comblike polymer systems,[32,78−81] or may be baseline artifacts. The first possibility was tested by subjecting various samples to lengthy annealing at temperatures a little below weak DSC events. For the fifth phenol-type 10Q complex, NC−O10Q/PSS, weak birefringence was visible after 1−2 h of annealing a few degrees below the DSC event at ca. 120 °C and was reversible on cycling above and below this event. Similarly, some weak birefringence developed in O_2N-N(Me)10Q/PSS after annealing for 1−2 days at ca. 100 °C; it vanished above the weak DSC event near 120 °C and again required lengthy annealing at 100 °C to reappear. These experiments indicate that the weak DSC event in these two complexes reflects a real transition, but involving a poorly or partially developed mesophase. In contrast, annealing of O_2N-N(Et)10Q/PSS and NC−N(Et)10Q/PSS at 100−105 °C (below slight hints of DSC events) for 3 days did not result in birefringence.

The only 6Q complex that shows a clear peak in DSC but no birefringence in POM, O_2N-N(Me)6Q/PSS, was found to develop birefringence after annealing at 140 °C (weak after 2−3 h, clearer after 1 day; reversible on cycling around the DSC transition at 155 °C). O_2N-O6Q/PSS (for which a slight hint of weak DSC events appear near 130 and 155 °C that are possibly very weak versions of the two events/peaks for the 10Q analogue) actually showed hints of birefringence in the as-prepared sample, which disappeared at ca. 150 °C (reversible in some conditions), but we were unable to produce any clear birefringence by annealing. Birefringence was not observed in O_2N-N(Et)6Q/PSS, NC−O6Q/PSS, or H−O6Q/PSS after annealing at 120 °C for a day, 115 °C for a day, and 100 °C for 6 days, respectively, all at temperatures a little below slight hints of DSC events (annealing experiments were not conducted on H_3CO-O6Q/PSS and H_3C-O6Q/PSS). It is recognized, however, that annealing at another temperature and/or for longer times might perhaps develop birefringence in one or more of these samples.

To summarize the POM experiments, not only is it virtually impossible to obtain revelatory textures for the complexes that show birefringence (except by recourse to a solvent technique), but it can be difficult to obtain birefringence

at all in other complexes without considerable patience. This makes it somewhat problematic to distinguish complexes that are intrinsically isotropic from those that are intrinsically liquid crystalline but that have frozen-in isotropic morphology.

Molecular Order in the SM/PSS Complexes. More direct information about the state of order in the complexes can be obtained by XRD. The POM experiments described above indicate that annealing is necessary to favor an equilibrium state in these complexes. Imrie and colleagues reported that (short) annealing was necessary to obtain reliable XRD data for all-covalent PS-based SCLCPs as well.[50] Figure 3 thus gives the diffractograms of the 6Q/PSS and 10Q/PSS complexes taken at ambient temperature after annealing at elevated temperatures for generally long times. The angles of the diffraction peak maxima and associated Bragg spacings are given in Table 4. A diffractogram of the parent PSS−Na is also shown in Figure 3 for comparison. It displays a fairly broad, distinct maximum centered at 4.7° corresponding to a Bragg spacing of 18.8 Å, which compares well with the calculated diameter of 19.6 Å for the PSS−Na chain (assuming random distribution of the styrenesulfonate moieties around the polymer backbone); this peak can therefore be ascribed to the average center-to-center distance of closest approach of neighboring PSS−Na chains in the amorphous state.

Before discussing the diffractograms of the annealed complexes, it should be mentioned that the four 10Q/PSS complexes that were birefringent in POM and that showed a clear DSC peak showed little or no evidence of order, according to XRD, in their as-prepared form. However, one or more XRD peaks in the lower-angle region (three for H_3CO−O10Q/PSS) developed during the initial stepwise heating scan at temperatures well above the T_g, as shown in the Supporting Information for O_2N−O10Q/PSS. Annealing tended to improve the order to some extent (somewhat sharper and more intense peaks) but did not change the nature of the order (unchanged peak positions). In contrast, O_2N−N(Me)6Q/PSS, although it gave a clear DSC peak, showed no evidence of order by XRD until it was subjected to lengthy annealing (see below). Some other complexes, specified below, also developed long-range order after lengthy annealing, whereas still others underwent little or no change. Whether annealed or not, the wide-angle region features only a broad halo, associated with the disordered nature of the ionically complexed side chains.

Regarding the XRD of the annealed samples in Figure 3 and focusing first on the 10Q/PSS series, two basic patterns can be observed in the low-angle region. The first one is shown by the three complexes with nonpolar terminal groups ("nonpolar-tailed complexes"). They all display three equidistant diffraction peaks in order of decreasing intensity, which, combined with the wide-angle halo, is a typical pattern observed for lamellar order of the SmA and SmC types. The peaks are the sharpest and best defined for H_3CO−O10Q/PSS, which also possesses the highest isotropization enthalpy in DSC and the most intense birefringence in POM. The corresponding Bragg spacings indicate a layer thickness of 34−35 Å for these complexes.

The second pattern is shown by the two phenol-type complexes, O_2N−O10Q/PSS and NC−O10Q/PSS, and the aniline-type complex with the smallest lateral substituent, O_2N−N(Me)10Q/PSS, all with polar terminal groups ("polar-tailed complexes"). These three complexes show a primary diffraction peak at ca. 4.5°, corresponding to a Bragg spacing of 19−20 Å. This peak is particularly intense for O_2N−N(Me)10Q/PSS (with a second peak at half the Bragg spacing weakly visible as well), but only after lengthy annealing. It is also relatively intense for O_2N−O10Q/PSS, which was subjected to stepwise heating/cooling cycles only (limited effective annealing),[72] whereas it is the weakest and broadest for NC−O10Q/PSS despite lengthy annealing. As discussed previously for O_2N−O10Q/PSS,[32] this peak may be a second-order diffraction from lamellar-type periodicity. In this case, the lamellar thickness for these complexes is 38−40 Å, larger than that for the nonpolar-tailed complexes above. It is noteworthy that Crivello et al. observed a weak first-order and sharp second-order peak for an NC−O azo mesogen covalently bound by an alkyl spacer (n=4, 6, 8, 10) to a poly(α-methylstyrene) backbone.[58] The extinction or reduction in intensity of the first-order peak is regularly reported in the literature (see, for example, refs 25, 78, and 82−84) and is generally attributed to an additional plane of electron density within the layers.[82] The appearance of LC order in O_2N−N(Me)10Q/PSS and NC−O10Q/PSS supports the attribution of the weak peaks observed in their DSC thermograms to the clearing temperature of a poorly developed LC phase.

The diffractogram of O_2N−N(Et)10Q/PSS, which differs from O_2N−N(Me)10Q/PSS only by the lateral substituent (Et vs Me) on the amine linking group, indicates short-range (isotropic) order only for this complex, including after lengthy annealing at the same temperature as led to the long-range order for the Me analogue. This can be ascribed at least in part to the lateral ethyl group, which, being more voluminous than the lateral methyl group, can sterically hinder ordered molecular packing of the mesogenic groups. Interestingly, the weak and broad small-angle peak that is present for the Et analogue occurs at about the same position as the sharp peak for the Me analogue, indicating a short-range tendency toward similar packing. The diffractogram of the CN-terminated aniline-type complex, which also possesses an Et substituent, shows a single weak and broad peak at low angles (Bragg spacing ca. 31.5 Å). Its position, which is closer to that for the nonpolar-tailed complexes, makes it an exception to the otherwise general distinction in the small-angle XRD pattern between the polar- and nonpolar-tailed 10Q/PSS complexes investigated. However, the unannealed form of the complex also shows this peak, and since neither POM nor DSC gives evidence of LC order in this complex, it can probably be ascribed to relatively short-range order in an otherwise isotropic state (observed also in some 6Q/PSS complexes and other systems; see below).

Of the 6Q/PSS complexes, only two were found to develop long-range order after appropriate annealing. We particularly investigated O_2N−N(Me)6Q/PSS, since it shows a DSC transition at 155 °C. First, it was found that 3 days of annealing at 130 °C resulted in little improvement in order; however, annealing at 140 °C (close to the DSC transition) for 2 days finally led to well-defined order (this also illustrates that the choice of annealing temperature can be critical): as shown in Figure 3, the first, second, and fourth (with a hint of the third) diffraction orders are apparent, with the second-order peak being the most intense, indicating a lamellar structure with a 35 Å periodicity. The periodicity and basic low-angle pattern are the same as for the polar-tailed 10Q/PSS complexes, taking into account the spacer-length difference.

The second 6Q complex for which long-range order was obtained is O_2N−O6Q/PSS. In this case, two sharp peaks appeared after 54 h of annealing at 150 °C. The XRD pattern indicates similar packing as for O_2N−N(Me)6Q/PSS (although the first-order peak appears a little more intense

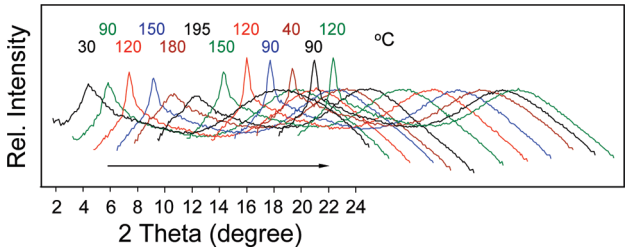

Figure 4. XRD of $O_2N-O10Q/PSS$ at various temperatures, where the curves are normalized relative to the WAXS halo and progressively shifted to the right in order of sequence of measurement relative to the as-prepared sample (30 °C). The position of the small-angle peak is essentially constant.[72]

than the second-order peak in this case), with a Bragg spacing of 36 Å. No long-range order was found in the other 6Q complexes after long-time annealing, where the annealing temperatures were chosen to be a little below hints of DSC events when possible (arbitrary temperatures were chosen otherwise).

It may be noted that H_3C-O6Q/PSS shows a relatively intense and broad peak at 2.52° (35 Å), which is unchanged from what was observed for the as-prepared sample. This could be related to short-range order in the isotropic state, as was observed also for some other ion-containing SCLCP polymers with nonpolar side-chain terminal groups.[25,75] It may be added that the lowest angle peak in the smectic phase of $H_3C-O10Q/PSS$ and $H-O10Q/PSS$ remains present in the isotropic phase of these complexes. This might be explained by the tendency for the ionic groups to aggregate in the isotropic state when in a less polar environment, thus forming short-range (possibly lamellar-like) structures; on the other hand, only some of the nonpolar-tailed complexes and one polar-tailed complex [NC−N(Et)10Q/PSS] in the series studied show this effect.

Regarding the evolution of the XRD diffractograms with temperature, it was noted that, apart from the annealing effects described above, the type of molecular packing structure and the Bragg spacings are essentially constant up to isotropization. Generally, the wide-angle halo moves to lower angles with increasing temperature (as expected for SmA mesophases), reflecting greater average lateral distances between the SM molecules due to increased thermal motion. A particular phenomenon, shown in Figure 4, was observed for $O_2N-O10Q/PSS$: the small-angle peak, which initially narrows in width and increases in intensity due to the annealing effect (three left-most curves in Figure 4), shows a partly *reversible* increase in intensity from ambient to 120 °C or more in the subsequent cooling−heating cycle (five rightmost curves in Figure 4; the decreased intensity at 150 °C is related to the proximity of T_{cl}). It is noteworthy that this intensity increase terminates in the temperature range of a weak and broad DSC event (ca. 120−140 °C), which had previously been hypothesized to be a second T_g-like transition;[32] however, its interpretation is not clear. A technique such as dynamic mechanical analysis might allow a better understanding of this unusual behavior in $O_2N-O10Q/PSS$ (with which its anomalously low T_g might also be associated).

It was noted above that the Bragg spacings of the complexes with LC order depend on the polarity of the SM tail, those for nonpolar tails being ca. 5 Å shorter than those for polar tails (at the same spacer length, and considering the primary diffraction peak as second-order for the latter). A similar dependence of the Bragg spacing on the polarity of the mesogen tail was observed for analogous all-covalent polystyrene-based SCLCPs (with butyl and octyl spacers)

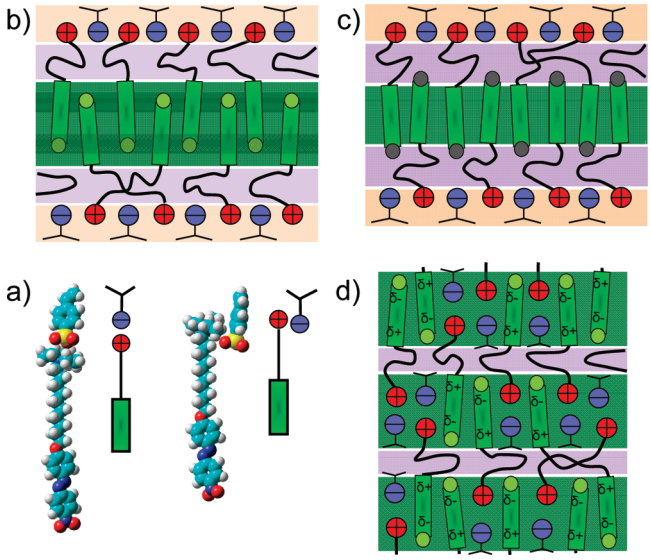

Figure 5. Schematics of possible packing models for the SM/PSS complexes with a SmA mesophase (see text for details).

studied by Imrie and colleagues: specifically, they observed that the Bragg spacings for SCLCPs with a H_3CO-O azo core are smaller than those for SCLCPs with O_2N-O and $NC-O$ azo cores.[50,62] (In addition, the enthalpy and entropy of the clearing transition are higher for the former than for the latter, as observed also in our complexes.) Assuming antiparallel side-by-side packing of the mesogens, these data were attributed to greater interdigitation of the rigid mesogenic cores with a nonpolar tail compared to those with a polar tail. This allows the nonpolar tail to lie in the same subplane as the alkyl spacer with which it is more miscible, whereas the polar tail lies in the same subplane as the rigid core with which it is more miscible (see further discussion below in relation to Figure 5). (This greater mesogenic overlap was also considered to account for the difference in enthalpies/entropies).[50,62]

In comparing the all-covalent PS-based SCLCP Bragg spacings (d) to calculated molecular lengths (l) with and without the backbone moiety included (d being a little lower and a little higher than l for the nonpolar- and polar-tailed SCLCPs, respectively, when the backbone moiety is included), Imrie and colleagues concluded that the polystyrene backbone was confined between the lamellar planes for the polar-tailed SCLCPs but was miscible with the side chains ("isotropic conformation" of the backbone) for the nonpolar-tailed SCLCPs.[50,62] In the present complexes, significant three-dimensional meandering of the backbone seems unlikely, since the driving force for nanophase separation between the ionic groups (directly connected to the PS backbone) and the neighboring alkyl spacers must be very strong. On the other hand, the ionic bonds in the complexes, being nondirectional bonds (although subject to the steric constraints imposed by the neighboring moieties), allow consideration of another possibility. Namely, there may be two distinct arrangements of the oppositely charged ionic groups within the molecular packing order: one where they are positioned approximately serially along the molecular long axis and another where they are positioned approximately side-by-side relative to the molecular long axis (Figure 5a). The all-trans molecular lengths given by the two arrangements were determined by Hyperchem to be ca. 40 and 35 Å, respectively, for the 10Q complexes and 35 and 30 Å, respectively, for the 6Q complexes (Table 4).

Comparison of these lengths with the experimental spacings (Table 4) suggests that this packing consideration is another way to rationalize the difference in Bragg spacings between the polar- and nonpolar-tailed complexes.

In light of the above discussion, various molecular models can be proposed for the apparently single-layer SmA packing structure of the SM/PSS complexes. Among the most straightforward models are the two illustrated in Figure 5b,c, where the mesogenic cores are interdigitated in antiparallel fashion. This arrangement is frequently proposed for SCLCPs in general, supposing that the side chains orient nonpreferentially on either side of the polymer backbone. The two groups of complexes are distinguished by greater interdigitation of the nonpolar-tailed mesogens (Figure 5c) than of the polar-tailed ones (Figure 5b), in line with what was proposed by Imrie and colleagues.[50,62] With the side-by-side overlapping of the mesogenic cores (and matching side-by-side alignment of the ionic groups), the alkyl chains fill in a lateral space equivalent to about two mesogenic molecular areas, thereby accounting for a lamellar thickness equivalent to a single effective side-chain length (see also refs 32 and 84). It is less clear how these models can account for the quasi-extinction of the first-order diffraction peak in one group of complexes and not in the other, unless it is related to the changes in the electron density profile of the mesogenic core region caused by the polar tails that are "just right" to result in extinction or partial extinction.

There is another possible source of extinction, as follows. The azo mesogens with higher dipole moments (those with polar end groups; Table 1) may be subject to electrostatic interactions with the ion pairs, which also form dipoles, with the result that ion pairs and mesogenic cores may be located in the same subplanes. Such an arrangement would reduce the effective lamellar thickness by half and thus rationalize the "second-order" diffraction peak, which, in this situation, is actually a first-order peak. A model illustrating the proposed arrangement is shown in Figure 5d. For adequate dipole−dipole interactions between ion pairs and mesogens, the ion pairs should be arranged serially relative to the molecular long axis. Within a subplane, the ion pairs may appear in sequences of variable lengths ranging from single to multiple ion pairs, which in turn are laterally interspersed between single to multiple sequences of mesogenic cores. In this case, and compared to the model in Figure 5c, the 5 Å difference in lamellar spacing between the polar- and nonpolar-tailed mesogens would appear to be related to the difference in ion pair arrangement rather than to the extent of mesogen interdigitation. However, the neat single or double rows of ion pairs in the idealized models may not reflect the true situation, especially considering the atactic nature of the polymer backbone combined with the disordered nature of SmA mesophases. Instead, the ion pairs may be arranged with variable local orientations (along with the mesogen cores), with the alkyl spacers allowing the necessary flexibility for adaption to lamellar order. From this perspective, the difference in mesogen interdigitation can once again be proffered as the best explanation for the ~5 Å difference in lamellar spacing between the polar- and nonpolar-tailed complexes. This is also consistent with the similar observation in the analogous all-covalent PS-based SCLCPs, for which the model of Figure 5d seems less applicable, and indeed, only a single diffraction peak (assumed to be first order) is reported for these SCLCPs. On the other hand, Figure 5d may be applicable to ion-containing SCLCP polymers described by Guillon and colleagues,[84] where biphenyl mesogenic groups are covalently attached through alkyl spacers to quaternized backbones. These polymers similarly organize as a single-layer smectic A mesophase

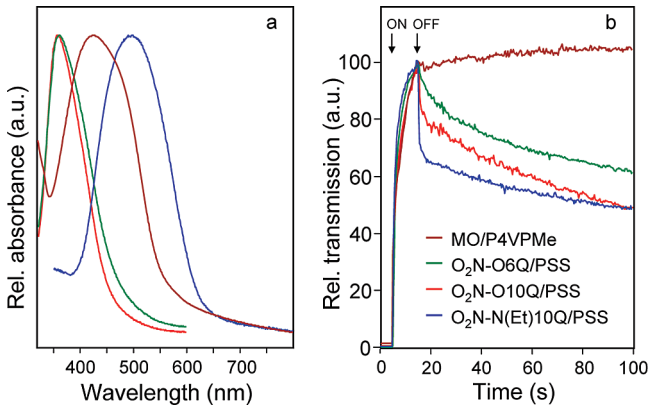

Figure 6. (a) UV−vis spectra and (b) photoinduced birefringence, relative to the maximum achieved at the end of the writing period, of spin-coated films of the complexes indicated in (b). The writing period in (b) takes place between the points marked as laser ON and laser OFF.

and give a second-order X-ray diffraction peak similar in intensity to the first-order one. The presence of both peaks in these cases, observed also in the two 6Q/PSS complexes showing LC order, might be explained by a higher proportion of longer sequences of ion pairs and mesogens within the sublayers.

SCLCP polymers can actually be thought of as trimer block molecules, where the three blocks correspond to (a) the rigid mesogenic core, (b) the alkyl spacer, and (c) the (ionic) polymer backbone.[51,63,85] From this point of view, the nonpolar-tailed complexes modeled essentially by Figure 5c can be described as a lamellar structure where the three blocks are segregated into three distinct subplanes, whereas the polar-tailed complexes modeled by Figure 5d can be described as a lamellar structure where block (a) and block (c) are located in the same subplanes. To investigate the validity of the proposed models, small-angle neutron scattering on appropriately deuterated samples or spectroscopic techniques that are sufficiently sensitive to local environments of specific atoms or groups (e.g., solid-state NMR, EXAFS, fluorescence) might be envisaged.

Photoinduced Birefringence (PIB) in Selected SM/PSS Complexes. Photoinduced birefringence is one often studied photonic property in photosensitive materials. We reported recently on the high and thermally stable photoinduced birefringence observed in a film composed of an equimolar ionic polymer complex of readily available methyl orange (MO) with methylated poly(4-vinylpyridine) (P4VPMe).[9] This impressive birefringence was attributed, at least partly, to the absence of flexible components such as a flexible spacer, combined with the ionic and polymeric nature of the complex and possibly its LC (smectic A) character. The effect of the flexible spacer can be qualitatively assessed by comparing the PIB of the present complexes with that of the spacer-free MO/P4VPMe complex.

The UV−vis spectra of spin-coated films of three SM/PSS complexes are shown in Figure 6a. The two O_2N−O*n*Q/PSS films both show a strong absorbance band centered at 360 ± 1 nm (with a slight shoulder near 400 nm), compared to 372 nm in H_2O for O_2N−O10Q,[72] ca. 375 nm for a similar complex of O_2N−O12Q with carboxymethylcellulose in chloroform,[36] and ca. 370 nm for this same complex in the form of ultrathin Langmuir−Blodgett films.[36] This band can be attributed to the azobenzene $\pi-\pi^*$ transition, which in the spin-coated film undergoes a blue shift, generally attributed to H-aggregation (side-by-side alignment of transition dipoles),[86,87] which is consistent with lamellar-type packing.[88]

The $O_2N-N(Et)10Q/PSS$ film shows a symmetric $\pi-\pi^*$ band at much higher wavelengths, centered at 497 nm, as is typical for azobenzenes substituted at the 4- and 4′-positions by an electron-donor and an electron-acceptor moiety, respectively (pseudo-stilbene type azo).[3] The spacer-free complex has a maximum absorbance at 425 nm, with a distinct shoulder on the high wavenumber side.

The room-temperature PIB curves of the three SM/PSS complexes compared with the spacer-free complex, normalized to the maximum PIB values obtained at the end of the writing period, are given in Figure 6b. It must be emphasized that all four complexes are stoichiometric, and they all involve similar ionic groups, in particular the strongly interacting sulfonate group, although the positive and negative moieties are inverted in the three SM/PSS complexes compared to MO/P4VPMe. While the spacer-free complex shows no relaxation of the PIB at all in the time period sampled after the writing laser is removed, all three SM/PSS complexes show a significant amount of fast relaxation, more for the decyl spacer than for the hexyl spacer, followed by much slower relaxation. This indicates that the flexible spacer is an important source of PIB relaxation. It may be caused, in part, by its plasticizing effect on the T_g. However, this cannot be the only factor, since the fast relaxation becomes more pronounced in the order $O_2N-O6Q/PSS < O_2N-O10Q/PSS < O_2N-N(Et)10Q/PSS$ whereas the T_g decreases in the order O_2N-O6Q/PSS (80 °C) > $O_2N-N(Et)10Q/PSS$ (68 °C) ≫ $O_2N-O10Q/PSS$ (46 °C). An additional factor may be the molecular packing: as shown earlier, $O_2N-N(Et)10Q/PSS$ is completely amorphous, whereas $O_2N-O10Q/PSS$ (like MO/P4VPMe[9]) has smectic A packing (although it is not known to what extent this packing actually exists in the spin-coated film), suggesting that LC structure contributes to reducing fast relaxation. Finally, it is noted that significant PIB, despite the presence of a flexible spacer, is nevertheless maintained at longer times, which can be related to the ionic and polymeric nature of the complexes. Further investigations of PIB and other photoinduced properties that illustrate clearly the effect of the presence of flexible moieties are described in a forthcoming paper on a series of spacer-free complexes.[89]

Concluding Remarks

The use of strongly interacting ionic functionalities of opposite charges constitutes an attractive means for constructing robust supramolecular SCLCPs that are stable to high temperatures. By contrast, hydrogen-bonding interactions are more attractive for supramolecular SCLCPs where greater temperature-dependent lability of the supramolecular bond is desired. However, the latter are more susceptible to partial complexation of the polymer backbone, even to the point of precluding the possibility of obtaining LC character in some cases.[44,45] Strong ionic bonding easily leads to equimolar complexation and thus to fully functionalized SCLCP homopolymers. Their downsides are a greater susceptibility to the effects of humidity and to nonequilibrium morphologies that can be difficult to erase.

In this paper, we have taken great care to avoid contamination by humidity as much as possible. This care, coupled with the greater inherent rigidity of the PS backbone and its relatively high molecular weight, has resulted in highly viscous materials that typically require exceedingly long annealing times at well-chosen temperatures to attain equilibrium morphologies. That is, many of the as-prepared complexes are amorphous or show relatively short-range LC-type order only, with true LC character revealed only after appropriate annealing. This can be understood in relation to polymer viscoelastic properties. To achieve equilibrium morphologies, the polymer chains must undergo translational motion, which occurs only in the presence of flow. It is well-known that increasing molecular weight raises the onset temperature for flow and increases the (temperature-dependent) flow viscosity and that ionic interactions exacerbate this effect drastically.[46] Thus, annealing must take place at temperatures that are much higher than the T_g to be effective (the higher the temperature, the lower the viscosity and therefore the faster the kinetics of chain movement), yet that are below any potential isotropization temperature. The slow kinetics of molecular reorganization suggests, moreover, that these systems are subject to partial development of LC order. This partial LC order can be in the form of both paracrystalline and positional disorder (limited correlation lengths), but it might also be in the form of variability in the extent of order throughout the sample (microheterogeneity).[90] Frequent crossover of polymer chains between sublayers can contribute significantly to this disorder.

Despite the above difficulties, the present investigation has shown a number of correlations between molecular parameters and LC properties. The T_g's of the complexes not only are spacer length dependent but also show an approximate correlation with the dipole moments of the mesogenic cores and, more specifically, with particular molecular aspects. In general, there are more 10Q than 6Q complexes that show LC order, as might be expected from longer side chains that can promote more effective nanophase separation. Only the aniline-type 10Q complexes with a lateral Et substituent appear to be intrinsically amorphous, which can be attributed to steric hindrance to efficient molecular packing caused by the Et branch. The spacer length of the 6Q complexes may be at the limit of that required to satisfy at once the packing tendencies of the mesogenic cores, the association of the interacting ionic groups, and the conformational tendencies of the polymer backbone, as seemed to be the case also in some other ion-containing SCLCPs.[48,75,91] When LC order is present, it is of the SmA type (but with distinctive characteristics depending on the mesogen type), which is the most frequently observed mesophase in ionic complexes and in ion-containing SCLCPs in general.[9,18,28−32,48,75,84,92]

By comparison, many all-covalent (nonionic) SCLCPs with alkyl spacer lengths less than $n = 6$ can resolve conflicting packing tendencies by adopting nematic order, a state which seems unlikely for ion-containing side-chain polymers given the strong driving force for nanophase separation between ionic and nonpolar motifs; they therefore remain amorphous if smectic order is no longer favorable. On the other hand, the all-covalent PS-based SCLCPs (analogous to the present complexes), which do not contain ionic groups, are LC (SmA) for spacers as short as *n*-propyl with the O_2N-O mesogenic core and *n*-butyl with the H_3CO-O and $NC-O$ mesogenic cores (but amorphous for H_3CO-O with the *n*-propyl spacer).[50,61,63] It may therefore also be argued that, in the ionic complexes, the *n*-hexyl spacer has less internal plasticization power (higher T_g and presumably a higher temperature of flow onset) than the *n*-decyl spacer, which may make it more difficult to find suitable annealing conditions (even impossible if the potential isotropization temperature is not sufficiently far from the T_g). Of the complexes for which some extent of LC order was achieved, there is no clear dependence of the isotropization temperature on specific molecular parameters. However, this tends to be general for liquid crystals, where transitions between phases depend sensitively on a combination of steric and polar factors. In the present case, this transition may, in addition, decrease in temperature and enthalpy when the LC order is poorly developed.

Finally, it is striking that a systematic difference was observed in the XRD pattern for the complexes with polar versus nonpolar mesogen tails, indicative of a systematic difference in the details of the lamellar packing. A possible

rationalization is that dipole−dipole interactions between the polar mesogenic cores and the ion pairs can result in both moieties sharing the same subplanes, thus reducing the effective lamellar periodicity by about half. The accompanying difference in Bragg spacing matches a similar difference in analogous all-covalent PS-based SCLCPs, suggestive of a general phenomenon.[50]

Acknowledgment. The financial support of NSERC Canada and FQRNT Québec is gratefully acknowledged. Dr. Ximin Chen is thanked for participating in the synthesis of some of the SMs. Prof. Christopher J. Barrett (Chemistry Dept., McGill University, Montreal) is thanked for making available his laboratory for PIB measurements, and Oleh Tanchak (former Ph.D. student in the Barrett laboratory) is thanked for training QZ in PIB investigations.

Supporting Information Available: Synthesis of representative SMs; NMR and elemental analysis of the SMs and complexes; TGA and DSC thermograms and X-ray diffractograms of the SMs; single crystal data for two SMs; conductivity measurements at end of dialysis for selected complexes; study of effects of dialysis time; TGA thermograms of the complexes; comparative T_g data; XRD as a function of temperature for O_2N−O10Q/PSS. This material is available free of charge via the Internet at http://pubs.acs.org.

References and Notes

(1) Natansohn, A.; Rochon, P. *Chem. Rev.* **2002**, *102*, 4139–4175.
(2) (a) Ikeda, T.; Mamiya, J.-i.; Yu, Y. *Angew. Chem., Int. Ed.* **2007**, *46*, 506–528. (b) Ikeda, T. *J. Mater. Chem.* **2003**, *13*, 2037–2057. (c) Barrett, C. J.; Mamiya, J.-i.; Yager, K. G.; Ikeda, T. *Soft Matter* **2007**, *3*, 1249–1261.
(3) Yager, K. G.; Barrett, C. J. In *Polymeric Nanostructures and Their Applications*; Nalwa, H. S., Ed.; American Scientific Publishers: Los Angeles, 2007; Vol. 2, pp 243−280.
(4) Yesodha, S. K.; Sadashiva Pillai, C. K.; Tsutsumi, N. *Prog. Polym. Sci.* **2004**, *29*, 45–74.
(5) Kajzar, F.; Lee, K.-S.; Jen, A. K.-Y. *Adv. Polym. Sci.* **2003**, *161*, 1–85.
(6) Advincula, R. C. In *Handbook of Polyelectrolytes and Their Applications*; Tripathy, S. K., Kumar, J., Nalwa, H. S., Eds.; American Scientific: Stevenson Ranch, CA, 2002; Vol. 1, pp 65−97.
(7) Yu, Y.; Nakano, M.; Ikeda, T. *Nature (London)* **2003**, *425*, 145.
(8) Yamada, M.; Kondo, M.; Mamiya, J.-i.; Yu, Y.; Kinoshita, M.; Barrett, C. J.; Ikeda, T. *Angew. Chem., Int. Ed.* **2008**, *47*, 4986–4988.
(9) Zhang, Q.; Bazuin, C. G.; Barrett, C. J. *Chem. Mater.* **2008**, *20*, 29–31.
(10) (a) Priimagi, A.; Kaivola, M.; Rodriguez, F. J.; Kauranen, M. *Appl. Phys. Lett.* **2007**, *90*, 121103/1–121103/3. (b) Priimagi, A.; Cattaneo, S.; Ras, R. H. A.; Valkama, S.; Ikkala, O.; Kauranen, M. *Chem. Mater.* **2005**, *17*, 5798–5802. (c) Priimagi, A.; Vapaavuori, J.; Rodriguez, F. J.; Faul, C. F. J.; Heino, M. T.; Ikkala, O.; Kauranen, M.; Kaivola, M. *Chem. Mater.* **2008**, *20*, 6358–6363.
(11) Stumpe, J.; Goldenberg, L.; Kulikovska, O. Film forming material and preparation of surface relief and optically anisotropic structures by irradiating a film of the said material. WO2006024500, **2006**.
(12) Xiao, S.; Lu, X.; Lu, Q.; Su, B. *Macromolecules* **2008**, *41*, 3884–3892.
(13) Lin, H.-C.; Tsai, C.-M.; Huang, G.-H.; Tao, Y.-T. *Macromolecules* **2006**, *39*, 557–568.
(14) Cui, L.; Zhao, Y. *Chem. Mater.* **2004**, *16*, 2076–2082.
(15) Imrie, C. T. *Trends Polym. Sci.* **1995**, *3*, 22–29.
(16) Bazuin, C. G. In *Mechanical and Thermophysical Properties of Polymer Liquid Crystals*; Brostow, W., Ed.; Chapman and Hall: London, 1998; Vol. 3, pp 59−100.
(17) (a) Kato, T. *Struct. Bonding (Berlin)* **2000**, *96*, 95–146. (b) Kato, T.; Mizoshita, N.; Kishimoto, K. *Angew. Chem., Int. Ed.* **2006**, *45*, 38–68.
(18) Masson, P.; Guillon, D. *Mol. Cryst. Liq. Cryst.* **2001**, *362*, 313–346.
(19) Paleos, C. M.; Tsiourvas, D. *Liq. Cryst.* **2001**, *28*, 1127–1161.
(20) Faul, C. F. J.; Antonietti, M. *Adv. Mater.* **2003**, *15*, 673–683.
(21) Binnemans, K. *Chem. Rev.* **2005**, *105*, 4148–4204.
(22) Pollino, J. M.; Weck, M. *Chem. Soc. Rev.* **2005**, *34*, 193–207.
(23) de Wit, J.; van Ekenstein, G. A.; Polushkin, E.; Kvashnina, K.; Bras, W.; Ikkala, O.; ten Brinke, G. *Macromolecules* **2008**, *41*, 4200–4204.
(24) (a) Canilho, N.; Kasëmi, E.; Mezzenga, R.; Schlüter, A. D. *J. Am. Chem. Soc.* **2006**, *128*, 13998–13999. (b) Canilho, N.; Scholl, M.; Klok, H.-A.; Mezzenga, R. *Macromolecules* **2007**, *40*, 8374–8383.
(25) Sallenave, X.; Bazuin, C. G. *Macromolecules* **2007**, *40*, 5326–5336.
(26) Medvedev, A. V.; Barmatov, E. B.; Medvedev, A. S.; Shibaev, V. P.; Ivanov, S. A.; Kozlovsky, M.; Stumpe, J. *Macromolecules* **2005**, *38*, 2223–2229.
(27) Xu, J.; Toh, C. L.; Liu, X.; Wang, S.; He, C.; Lu, X. *Macromolecules* **2005**, *38*, 1684–1690.
(28) Ujiie, S.; Iimura, K. *Macromolecules* **1992**, *25*, 3174–3178.
(29) (a) Bazuin, C. G.; Tork, A. *Macromolecules* **1995**, *28*, 8877–8880. (b) Brandys, F. A.; Masson, P.; Guillon, D.; Bazuin, C. G. *Macromol. Chem. Phys.* **2001**, *202*, 856–865. (c) Tork, A.; Bazuin, C. G. *Macromolecules* **2001**, *34*, 7699–7706. (d) Bazuin, C. G.; Boivin, J.; Tork, A.; Tremblay, H.; Bravo-Grimaldo, E. *Macromolecules* **2002**, *35*, 6893–6899.
(30) Tal'roze, R. V.; Kuptsov, S. A.; Sycheva, T. I.; Bezborodov, V. S.; Platé, N. A. *Macromolecules* **1995**, *28*, 8689–8691.
(31) Gohy, J.-F.; Antoun, S.; Sobry, R.; Van den Bossche, G.; Jérôme, R. *Macromol. Chem. Phys.* **2000**, *201*, 31–41.
(32) Tibirna, C. M.; Bazuin, C. G. *J. Polym. Sci., Part B: Polym. Phys.* **2005**, *43*, 3421–3431.
(33) Benouazzane, M.; Bravo-Grimaldo, E.; Bissessur, R.; Bazuin, C. G. *Macromolecules* **2006**, *39*, 5364–5370.
(34) Goddard, E. D. In *Interactions of Surfactants with Polymers and Proteins*; Goddard, E. D., Ananthapadmanabhan, K. P., Eds.; CRC Press: Boca Raton, 1993; Chapter 4. Lindman, B.; Thalberg, K. Ibid., Chapter 5.
(35) Abdallah, D.; Cully, M. J.; Li, Y.; Shipp, D. A. *Colloid Polym. Sci.* **2008**, *286*, 739–745.
(36) (a) Panambur, G.; Robert, C.; Zhang, Y.; Bazuin, C. G.; Ritcey, A. M. *Langmuir* **2003**, *19*, 8859–8866. (b) Panambur, G.; Zhang, Y.; Yesayan, A.; Galstian, T.; Bazuin, C. G.; Ritcey, A. M. *Langmuir* **2004**, *20*, 3606–3615.
(37) (a) Kunitake, T.; Okahata, Y.; Shimomura, M.; Yasunami, S.; Takarabe, K. *J. Am. Chem. Soc.* **1981**, *103*, 5401–5413. (b) Tian, Y.; Umemura, J.; Takenaka, T.; Kunitake, T. *Langmuir* **1988**, *4*, 1064–1066. (c) Kunitake, T. *Angew. Chem., Int. Ed.* **1992**, *31*, 709–726.
(38) (a) Everaars, M. D.; Marcelis, A. T. M.; Sudhölter, E. J. R. *Liebigs Ann./Recl.* **1997**, 21–26. (b) Nieuwkerk, A. C.; Marcelis, A. T. M.; Koudijs, A.; Sudhölter, E. J. R. *Liebigs Ann./Recl.* **1997**, 1719–1724.
(39) Engelking, J.; Menzel, H. *Thin Solid Films* **1998**, *327−329*, 90–95.
(40) Caculitan, N. G.; Scudder, P. H.; Rodriguez, A.; Casson, J. L.; Wang, H.-L.; Robinson, J. M.; Johal, M. S. *Langmuir* **2004**, *20*, 8735–8739.
(41) (a) Navarro-Rodriguez, D.; Frère, Y.; Gramain, P.; Guillon, D.; Skoulios, A. *Liq. Cryst.* **1991**, *9*, 321–335. (b) Bravo-Grimaldo, E.; Navarro-Rodriguez, D.; Skoulios, A.; Guillon, D. *Liq. Cryst.* **1996**, *20*, 393–398. (c) Tittarelli, F.; Masson, P.; Skoulios, A. *Liq. Cryst.* **1997**, *22*, 721–726.
(42) Tschierske, C. *Prog. Polym. Sci.* **1996**, *21*, 775–852.
(43) Kawakami, T.; Kato, T. *Macromolecules* **1998**, *31*, 4475–4479.
(44) Brandys, F. A.; Bazuin, C. G. *Chem. Mater.* **1996**, *8*, 83–92.
(45) (a) Stewart, D.; Imrie, C. T. *Macromolecules* **1997**, *30*, 877–884. (b) Stewart, D.; Paterson, B. J.; Imrie, C. T. *Eur. Polym. J.* **1997**, *33*, 285–290. (c) Stewart, D.; Imrie, C. T. *J. Mater. Chem.* **1995**, *5*, 223–228.
(46) (a) Eisenberg, A.; King, M. *Ion-Containing Polymers*; Academic Press: New York, 1977. (b) Eisenberg, A.; Kim, J.-S. Introduction to Ionomers; John Wiley & Sons: New York, 1998.
(47) Zundel, G. *Hydration and Intermolecular Interaction*; Academic Press: New York, 1970.
(48) Vuillaume, P. Y.; Bazuin, C. G.; Galin, J.-C. *Macromolecules* **2000**, *33*, 781–790.
(49) In a follow-up paper, the influence of humidity and other solvent atmospheres on the LC structure of selected complexes will be described: Zhang, Q.; Bazuin, C. G., to be submitted.
(50) Imrie, C. T.; Schleeh, T.; Karasz, F. E.; Attard, G. S. *Macromolecules* **1993**, *26*, 539–544.
(51) Imrie, C. T.; Karasz, F. E.; Attard, G. S. *Macromolecules* **1993**, *26*, 3803–3810.

(52) Craig, A. A.; Imrie, C. T. *Macromolecules* **1995**, *28*, 3617–3624.
(53) Hamley, I. W.; Imrie, C. T. *J. Mater. Sci. Lett*. **1998**, *17*, 339–341.
(54) Bosshard, C.; Sutter, K.; Prêtre, P.; Hulliger, J.; Flörsheimer, M.; Kaatz, P.; Günter, P. *Organic Nonlinear Optical Materials*; Gordon and Breach Publishers: Basel, 1995.
(55) Prasad, P. N.; Williams, D. J. *Introduction to Nonlinear Optical Effects in Molecules and Polymers*; Wiley: New York, 1991.
(56) McArdle, C. B. *Side Chain Liquid Crystal Polymers*; Chapman and Hall: New York, 1989.
(57) Demus, D.; Goodby, J.; Gray, G. W.; Spiess, H.-W.; Vill, V. *Handbook of Liquid Crystals*; Wiley-VCH: Toronto, 1998; Vol. III.
(58) Crivello, J. V.; Deptolla, M.; Ringsdorf, H. *Liq. Cryst*. **1988**, *3*, 235–247.
(59) (a) McCulloch, I. A.; Bailey, R. T. *Proc. SPIE—Int. Soc. Opt. Eng*. **1990**, *1147*, 134–140. (b) McCulloch, I. A.; Bailey, R. T. *Mol. Cryst. Liq. Cryst*. **1991**, *200*, 157−165. Ref 57, p 258.
(60) Imrie, C. T.; Karasz, F. E.; Attard, G. S. *Liq. Cryst*. **1991**, *9*, 47–57.
(61) Imrie, C. T.; Karasz, F. E.; Attard, G. S. *Macromolecules* **1992**, *25*, 1278–1283.
(62) Schleeh, T.; Imrie, C. T.; Rice, D. M.; Karasz, F. E.; Attard, G. S. *J. Polym. Sci., Part A: Polym. Chem*. **1993**, *31*, 1859–1869.
(63) Imrie, C. T.; Karasz, F. E.; Attard, G. S. *Macromolecules* **1993**, *26*, 545–550.
(64) Imrie, C. T.; Karasz, F. E.; Attard, G. S. *Makromol. Chem., Rapid Commun*. **1993**, *14*, 351–357.
(65) Imrie, C. T.; Karasz, F. E.; Attard, G. S. *J. Macromol. Sci., Pure Appl. Chem*. **1994**, *A31*, 1221–1232.
(66) Imrie, C. T.; Karasz, F. E.; Attard, G. S. *Macromolecules* **1994**, *27*, 1578–1581.
(67) Ulman, A.; Willand, C. S.; Kohler, W.; Robello, D. R.; Williams, D. J.; Handley, L. *J. Am. Chem. Soc*. **1990**, *112*, 7083–7090.
(68) Vogel, A. I. *Vogel's Textbook of Practical Organic Chemistry, Including Qualitative Organic Analysis*; Longman: New York, 1978.
(69) Zollinger, H. *Azo and Diazo Chemistry: Aliphatic and Aromatic Compounds*; Interscience: New York, 1961.
(70) Heldmann, C.; Warner, M. *Macromolecules* **1998**, *31*, 3519–3531.
(71) Samyn, C.; Verbiest, T.; Kesters, E.; Van den Broeck, K.; Van Beylen, M.; Persoons, A. *Polymer* **2000**, *41*, 6049–6054.
(72) See Supporting Information.
(73) Antonietti, M.; Conrad, J.; Thünemann, A. *Macromolecules* **1994**, *27*, 6007–6011.
(74) Ponomarenko, E. A.; Tirrell, D. A.; MacKnight, W. J. *Macromolecules* **1996**, *29*, 8751–8758.
(75) Vuillaume, P. Y.; Sallenave, X.; Bazuin, C. G. *Macromolecules* **2006**, *39*, 8339–8346.
(76) Noël, C. In Ref 56.
(77) Wang, W.; Hashimoto, T. *Macromolecules* **1999**, *32*, 3163–3166.
(78) Vuillaume, P. Y.; Bazuin, C. G. *Macromolecules* **2003**, *36*, 6378–6388.
(79) Percec, V.; Hahn, B.; Ebert, M.; Wendorff, J. H. *Macromolecules* **1990**, *23*, 2092–2095.
(80) Emmerling, U.; Lindau, J.; Diele, S.; Werner, J.; Kresse, H. *Liq. Cryst*. **2000**, *27*, 1069–1073.
(81) (a) Hiller, S.; Pascui, O.; Budde, H.; Kabisch, O.; Reichert, D.; Beiner, M. *New J. Phys*. **2004**, *6*, 10. (b) Beiner, M.; Huth, H. *Nat. Mater*. **2003**, *2*, 595–599.
(82) Davidson, P. *Prog. Polym. Sci*. **1996**, *21*, 893–950.
(83) Nieuwhof, R. P.; Marcelis, A. T. M.; Sudhölter, E. J. R. *Macromol. Chem. Phys*. **1999**, *200*, 2494–2500.
(84) (a) Navarro-Rodriguez, D.; Guillon, D.; Skoulios, A.; Frère, Y.; Gramain, P. *Makromol. Chem*. **1992**, *193*, 3117–3128. (b) Masson, P.; Gramain, P.; Guillon, D. *Macromol. Chem. Phys*. **1995**, *196*, 3677–3686. (c) Masson, P.; Gramain, P.; Guillon, D. *Macromol. Chem. Phys*. **1999**, *200*, 616–620.
(85) Tschierske, C. *J. Mater. Chem*. **2001**, *11*, 2647–2671.
(86) Kasha, M. *Radiat. Res*. **1963**, *20*, 55–70.
(87) Hirano, Y.; Tokuoka, Y.; Kawashima, N.; Ozaki, Y. *Vib. Spectrosc*. **2007**, *43*, 86–96.
(88) Nieuwkerk, A. C.; Marcelis, A. T. M.; Koudijs, A.; Sudhölter, E. J. R. *Liebigs Ann./Recl*. **1997**, 1719–1724.
(89) Zhang, Q.; Wang, X.; Barrett, C. J.; Bazuin, C. G. *Chem. Mater*., in press.
(90) Tsukruk, V. V.; Shilov, V. V.; Lipatov, Y. S. *Acta Polym*. **1985**, *36*, 403–412.
(91) Köberle, P.; Laschewsky, A. *Macromolecules* **1994**, *27*, 2165–2173.
(92) (a) Ujiie, S.; Iimura, K. *Polym. J* **1993**, *25*, 347–354. (b) Ujiie, S.; Tanaka, Y.; Iimura, K. *Mol. Cryst. Liq. Cryst*. **1993**, *225*, 399−402 and *231*, 263−267. (c) Haramoto, Y.; Kusakabe, Y.; Nanasawa, M.; Ujiie, S.; Mang, S.; Schwarzwalder, C.; Holmes, A. B. *Liq. Cryst*. **2000**, *27*, 1393–1397.